Available online at www.sciencedirect.com
SCIENCE DIRECT®
Journal of Nuclear Materials 343 (2005) 285–296
journal of nuclear materials
www.elsevier.com/locate/jnucmat

Radiation hardening and -embrittlement due to He production in F82H steel irradiated at 250 °C in JMTR

E. Wakai [a,*], S. Jitsukawa [a], H. Tomita [b], K. Furuya [a], M. Sato [a], K. Oka [c], T. Tanaka [c], F. Takada [b], T. Yamamoto [b], Y. Kato [b], Y. Tayama [b], K. Shiba [a], S. Ohnuki [c]

[a] *Department of Materials Science, Japan Atomic Energy Research Institute, Tokai-mura, Ibaraki-ken, 319-1195, Japan*
[b] *Japan Atomic Energy Research Institute, Oarai-machi, Ibaraki-ken 311-1394, Japan*
[c] *Hokkaido University, Kita-ku, Sapporo 060-8628, Japan*

Abstract

The dependence of helium production on radiation hardening and -embrittlement has been examined in a reduced-activation martensitic F82H steel (8Cr–2W–0.2V–0.04Ta–0.1C) irradiated at 250 °C to 2.3 dpa. In this study, ^{10}B and ^{11}B-doped specimens were irradiated to minimize the errors from the effect of B on mechanical properties by comparing the results. The specimens used were ^{10}B-doped, ^{10}B + ^{11}B-doped and ^{11}B-doped F82H steels. The total amounts of doping boron were about 60 mass ppm. The range of helium concentration produced in the specimens was from about 5 to about 330 appm. Tensile and fracture toughness tests were performed after neutron irradiation. 50 MeV-He^{2+} irradiation was also performed to implant about 85 appm He atoms at 120 °C by AVF cyclotron to 0.03 dpa, and small punch testing was performed to obtain ductile-to-brittle transition temperatures (DBTT). Radiation hardening of the neutron-irradiated specimens increased slightly with increasing helium production. The 100 MPa $m^{1/2}$ DBTT for the F82H + ^{11}B, F82H + ^{10}B + ^{11}B, and F82H + ^{10}B specimens were 40, 110, and 155 °C, respectively. The shifts of DBTT due to helium production were evaluated as about 70 °C by 190 appm He and 115 °C by 330 appm He. In cyclotron experiment using standard F82H, a similar DBTT shift due to He was measured. These results suggest that helium production can increase the DBTT.

1. Introduction

Reduced-activation ferritic/martensitic steels are candidate materials for the vessel of liquid target of spallation neutron source and for blanket structure of fusion reactors. The structural materials must not only withstand radiation damage, but also accommodate helium atoms due to transmutation process. The effects of neutron irradiation on tensile deformation, DBTT, and microstructures of F82H and the other ferritic/martensitic steels were reported previously [1–13]. In fission data, radiation hardening occurred mainly at irradiation temperatures lower than about 400 °C, and it increased with decreasing irradiation temperature up to about 250 °C. The ductile to brittle transition temperature (DBTT) tended to increase with decreasing irradiation temperature, and the shift increased largely at 250 °C.

* Corresponding author. Tel.: +81 29 282 6563; fax: +81 29 282 5922.
E-mail address: wakai@realab01.tokai.jaeri.go.jp (E. Wakai).

0022-3115/$ - see front matter © 2005 Elsevier B.V. All rights reserved.
doi:10.1016/j.jnucmat.2004.10.167

It was reported that shifts of DBTT measured by Charpy impact and compact tension tests in F82H irradiated at 300 °C to 2–3 dpa by neutrons were almost the same as each other [10]. In spallation target data, the DBTT shift is little temperature dependent or even increases slightly in temperature range between 100 and 350 °C. The issue of helium accumulation on mechanical properties has been an ongoing concern. Recently, the effect of helium production on radiation hardening has been examined and a large enhancement of hardening due to helium from 600 appm to 5000 appm was detected in tensile testing on 9Cr martensitic steels EM10 and T91 implanted by cyclotron experiments [14,15]. Slight enhancement of radiation hardening was also reported in neutron irradiation experiments [16,17] and ion beam experiments [14,15,18–21]. It has been reported by several researchers that helium can enhance the DBTT shift [8–10]. The quantified analysis of the dependence of helium production on DBTT has not been examined. Radiation-induced degradation of fracture toughness related to helium production is recognized to be one of the critical issues of the alloys. Recently, the synergistic effects of helium, hydrogen and displacement damage have been reported for swelling behavior [22–24] and mechanical properties [25–31], and the synergistic effect has been an ongoing concern.

Many of spallation target data are recently reported, and the interpretation of mechanical properties of spallation target experiment is thought to be relatively complex, because the irradiation environment has several factors such as the levels of displacement damage, helium and hydrogen, and irradiation temperature. Our study, therefore, tried to extract the synergistic effect of displacement damage and helium including no hydrogen, and the behaviors of mechanical properties was analyzed. In order to quantify the dependence of helium production on DBTT and hardening, the isotope ^{10}B doping technique was used to produce He atoms in the alloys using a different ^{10}B concentration in a mixed spectrum reactor irradiation with thermal and first neutrons. Doping of the B element can affect the mechanical properties before and after irradiation, and the errors induced from the effect of B on mechanical properties have to be minimized by comparing the results of the mechanical testing of ^{10}B and ^{11}B-doped specimens. Alloys used in this study are F82H doped with ^{10}B, ^{10}B + ^{11}B and ^{11}B, respectively. The purpose of this study is focused to evaluate quantitatively the contribution of helium production on hardening and DBTT in F82H for the synergistic effect of helium and displacement damage.

2. Experimental procedure

2.1. Materials

The materials used in this study and the compositions are given in Table 1. In order to produce helium atoms the materials were doped with about 60 mass ppm ^{10}B. The purity of isotope elements of ^{10}B and ^{11}B used in this study was about 95%. 15 mm thick plates of these materials were normalized at 1040 °C for 40 min and tempered at 750 °C for 60 min.

0.18DCT, Charpy impact specimens and SS-3 specimens were used to evaluate the DBTT and hardening in this study. The 0.18DCT specimens (12.5 mm diameter and 4.63 mm thickness) were machined in the T–L orientation so that crack propagation occurred parallel to the rolling direction. Fatigue pre-cracking was performed at room temperature in a condition of crack length to specimen width ratio (a/W) of approximately 0.46. This was followed by side-grooving on each side to depth of ~10% of specimen thickness. Half-size Charpy impact specimens (5 mm width, 10 mm height, 50 mm length) with V-notches were also used for the measurement of DBTT and were produced parallel to the rolling direction (L–T) of the material plates. The SS-3 tensile specimens were 0.76 mm thick with a gage length of 7.6 mm as shown in Fig. 1(a) and were also taken parallel to the rolling direction.

2.2. Irradiation conditions

Irradiation was carried out at nominally 250 °C in the capsule 00M-66A of the Japan Materials Test Reactor (JMTR) in the Japan Atomic Energy Research Institute (JAERI) to neutron fluences of 1.4×10^{21} n/cm^2 ($E > 1$ MeV) and 1.2×10^{21} n/cm^2 ($E < 0.683$ eV), resulting in a displacement damage of ~ 2.2 dpa. The averaged displacement damage induced by the reaction of $^{10}\mathrm{B}(n,\alpha)^7\mathrm{Li}$ was calculated as about 0.2 and 0.1 dpa for the F82H + ^{10}B and F82H + ^{11}B + ^{10}B, respectively. The total displacement damage due to the transmutation reaction and neutron irradiation was 2.4 dpa in the F82H + ^{10}B.

Table 1
Chemical compositions of materials (mass%)

Materials	B	C	Si	Mn	P	S	Cr	W	V	Ta
F82H + ^{10}B	0.0061	0.097	0.10	0.10	0.007	0.001	7.96	1.98	0.18	0.05
F82H + ^{11}B	0.0059	0.093	0.11	0.10	0.007	0.001	8.02	1.98	0.18	0.05
F82H + ^{10}B + ^{11}B	0.0067	0.094	0.12	0.90	0.007	0.001	8.01	2.01	0.18	0.05

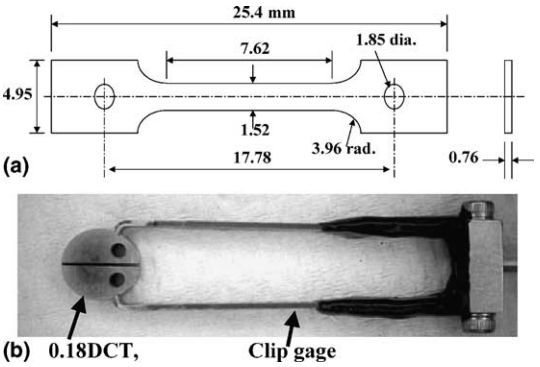

Fig. 1. (a) Tensile specimen of SS-3 type, (b) the outboard clip gage seated on the disk compact specimen.

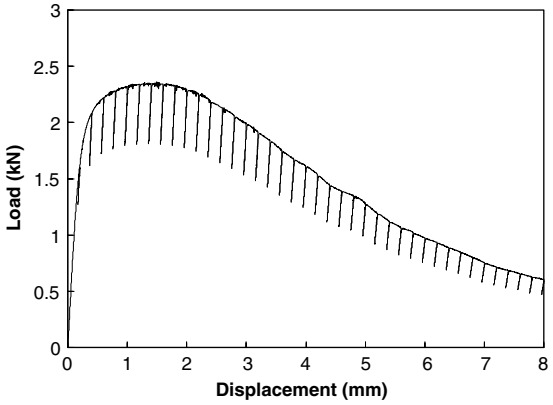

Fig. 2. Load and displacement curve for unloading compliance method to detect crack growth.

The TEM disk specimens of 0.3 mm thickness were implanted at about 120 °C with a beam of 50 MeV-He^{2+} particles by AVF cyclotron at TIARA facility of JAERI. An energy degrader was used to implant helium into the specimens from top to bottom uniformly [32]. The concentration of the He and displacement damage in the specimen implanted by cyclotron irradiation was evaluated as about 85 appm He and 0.03 dpa, respectively. The purpose of this helium implantation experiment using F82H-std specimens is to evaluate the effect of helium production on DBTT and to eliminate the effect of transmutation atom of lithium, produced by the reaction of $^{10}B(n,\alpha)^7$ Li using the F82H + ^{10}B specimen, on the shift of DBTT.

2.3. Testing conditions

After neutron irradiation, fracture toughness and tensile tests were performed. *J*-integral resistance curves were determined using an unloading compliance technique in general accordance with the ASTM E 813-89 – Standard Test Method for J_{IC}. In brittle regime and in the transition regime, ASTM E399 K_{IC} procedure was performed. Fig. 1(b) shows the outboard gage attached to one of the disk compact specimens. Fracture toughness tests were conducted in the temperature range from −130 to 310 °C, and the temperatures were controlled by LN_2 vapor and electric heaters. Tensile force, clip gage displacement, cross head displacement and temperature were measured and recorded during the tests. Cross head displacement rate of 0.2 mm/min was selected. *J*-integrals were obtained from the load versus clip gage displacement curves as shown in Fig. 2. The temperature dependence of the effective fracture toughness was examined and DBTT was evaluated. Tensile testing was carried out in vacuum at a strain rate of 4×10^{-4}/s at 25, 250, and 400 °C. After the fracture testing, the fracture surface was observed by SEM and Cr, C and B distributions were mapped by auger electron spectroscopy at 20 kV.

Following the implantation, small punch (SP) tests were carried out at temperatures between −180 °C and 25 °C in a hot cell of the JMTR hot laboratory. The SP test machine consists of a load controller, turntable with twelve specimen holders, vacuum chamber and furnace. A cross-sectional view of the specimen holder in the SP test machine is shown in Fig. 3. The specimen holder consists of the upper and lower holders, punch and steel ball of 1 mm diameter. The steel ball and punch were pushed by the punch rod. The maximum load and stroke of the punch rod is 5 kN and 8 mm, respectively. The punch speed was controlled at 0.5 mm/min. SP energy was calculated from the area under the load–deflection curve up to the fracture load. The microstructures after the implantation were observed by a transmission electron microscope (TEM) operated at 200 kV in the Tokai hot

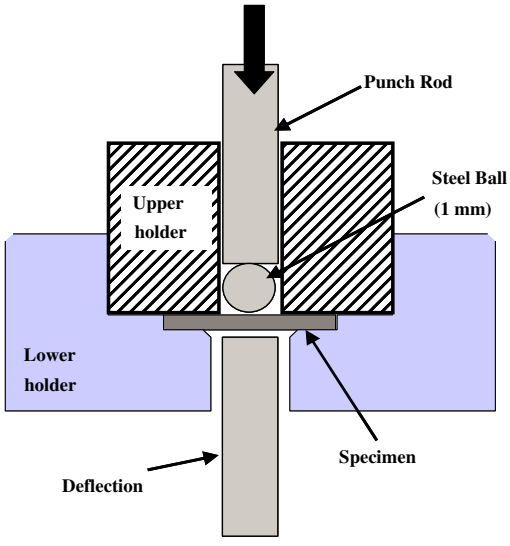

Fig. 3. Small punch testing machine and ϕ 3 mm specimen.

laboratory. After SP tests, the fracture surfaces were observed by a scanning electron microscope (SEM) in the JMTR hot laboratory.

2.4. He measurement

The concentrations of helium in the specimens after the irradiations were measured using a mass analyzer of magnetic reflection type. In this measurement, helium gas was released into the measurement system from the ion-implanted specimen after melting. In this technique, a known concentration of He gas is used for a standard relation between the gas intensity and concentration of He, as given in Fig. 4. The helium concentration in the F82H-std steel implanted by cyclotron irradiation was 84 appm, and helium concentrations produced from a reaction of $^{10}B(n,\alpha)^{7}Li$ in the F82H + B steels irradiated in the JMTR were evaluated and the range of helium concentration was from about 14 to 330 appm as shown in Table 2.

3. Results

3.1. Mechanical properties before irradiation

Tensile properties measured at 25 °C in the F82H + ^{10}B, F82H + ^{11}B, and F82H + ^{10}B + ^{11}B specimens before irradiation are given in Table 3. The tensile properties in these specimens are very similar to each other. In Charpy impact tests of non-irradiated specimens, the ductile–brittle transition temperatures of the F82H + ^{10}B, F82H + ^{11}B and F82H + ^{10}B + ^{11}B steels are −10, −5 and 5 °C, respectively. The upper shelf energy of these specimens was about 130 J.

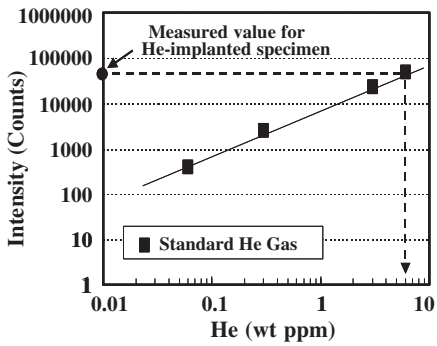

Fig. 4. He concentration measured by a mass analyzer of magnetic reflection type.

Table 2
He concentrations of the specimens used in this study

Materials	Irradiation	He (appm)
F82H-std	He implantation	84
F82H + ^{10}B	JMTR (neutron)	331
F82H + ^{11}B	JMTR (neutron)	14
F82H + ^{10}B + ^{11}B	JMTR (neutron)	194

The helium concentration was measured by using a mass analyzer of magnetic reflection type after melting treatment of the irradiated specimens.

3.2. Tensile testing after neutron irradiation

Tensile curves of F82H + ^{10}B, F82H + ^{11}B, and F82H + ^{10}B + ^{11}B specimens measured at 25 °C after irradiation were given in Fig. 5. The tensile properties of F82H + ^{10}B, F82H + ^{11}B, and F82H + ^{10}B + ^{11}B specimens before and after irradiation were given in Table 3. The increments of yield stress, ΔYS, and ultimate tensile strength, ΔUTS, are given in Fig. 6. In F82H + ^{10}B + ^{11}B and F82H + ^{10}B, ΔYS and ΔUTS increased somewhat with increasing helium production. This result shows that radiation hardening could be enhanced by helium production. The uniform and total elongations of the specimens after irradiation are presented in Fig. 7, and a large degradation of total elongation is observed in F82H + ^{10}B tested at 25 °C. This result indicates that uniform elongations in these irradiated materials are degraded by irradiation but are hardly affected by helium production, and the total elongations are hardly affected up to about 190 appm He, however it was degraded by about 330 appm helium production. The elongations in the irradiated specimens were recovered at 400 °C. The ratio of fracture strength to fracture area in tensile testing in the irradiated F82H + ^{10}B steel was about 40% smaller than that in the irradiated F82H + ^{11}B steel. The fracture strength in this study is simply defined as the ratio of stress to a cross-section of specimen in the necked region when fracture occurs. This result of 40% reduction might indicate that the fracture stress was reduced by a high amount of helium production.

3.3. Fracture testing after neutron irradiation

Fig. 8 shows the change of fracture toughness as a function of temperature in F82H + ^{11}B steel before and after irradiation. At low temperatures, large load drops occurred suddenly when the crack grew in a brittle regime. With elevating test temperature, the deformation behavior changed fracture into a ductile manner. For several specimens with high toughness, crack growth was evaluated by unloading compliance method. Crack began to grow at or close to the point of maximum load for most of the specimens. It is useful to characterize the transition temperatures indexed by toughness. While various indices could be chosen, fracture toughness is typically indexed at an elastic–plastic, cleavage-initiation level of 100 $MPa^{1/2}$ as shown by

Table 3
Summary of tensile properties of F82H + ^{10}B, F82H + ^{11}B and F82H + ^{10}B + ^{11}B steels irradiated at 250 °C to about 2.3 dpa in JMTR

Materials	Irradiation (dpa)	Test temperature (°C)	YS (MPa)	UTS (MPa)	UE (%)	TE (%)	RA (%)
F82H + ^{10}B	0	20	564	686	6.2	18.4	
	2.4	20	814	814	0.4	5.2	42
	0	250	483	467	2.7	12.6	
	2.4	250	641	649	0.4	8.1	69.7
	0	400	465	507	2.2	11.7	
	2.4	400	580	606	2.9	9.6	59.3
F82H + ^{11}B	0	20	552	679	6.1	17.4	
	2.2	20	719	727	0.3	10.2	82.7
	0	250	482	534	2.7	12	
	2.2	250	597	597	0.3	9.6	84.4
	0	400	460	493	2.2	11.8	
	2.2	400	545	563	2.5	12.6	78.4
F82H + ^{10}B + ^{11}B	0	20	589	702	5.7	16.1	
	2.3	20	814	814	0.4	8.5	73.2
	0	250	566	612	2.2	10.2	
	2.3	250	649	658	0.7	8.4	65.4
	0	400	498	529	1.8	10.8	
	2.3	400	571	589	2.1	10.1	62.8

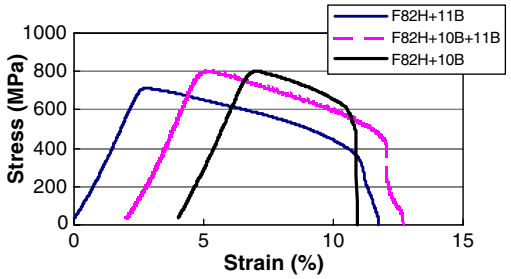

Fig. 5. Tensile curves of F82H + ^{11}B, F82H + ^{10}B + ^{11}B and F82H + ^{10}B specimens tested at room temperature after 250 °C irradiation of 2.3 dpa.

Lucas [33]. The 100 MPa $m^{1/2}$ transition temperatures for the non-irradiated and irradiated F82H + ^{11}B specimens were about −100 and 40 °C, respectively. The shift in DBTT caused by irradiation was about 140 °C and the shift of DBTT was caused mainly by displacement damage. The shifts of DBTT in the irradiated specimens are also shown in Fig. 9. The 100 MPa $m^{1/2}$ transition temperatures for the F82H + ^{11}B, F82H + ^{10}B + ^{11}B, and F82H + ^{10}B were 40, 110, and 155 °C, respectively. From the comparison of fracture toughness between F82H + ^{11}B and F82H + ^{10}B + ^{11}B, the shift of DBTT due to helium production of about 190 appm can be estimated as +70 °C. The similar comparison of F82H + ^{11}B and F82H + ^{10}B shows that the shift of DBTT due to helium production of 330 appm is about +115 °C. This result indicates that the shift of DBTT in the radiation-hardened specimens increases with increasing helium production.

It is interesting to note that fracture toughness was largely reduced in the irradiated F82H + ^{10}B at

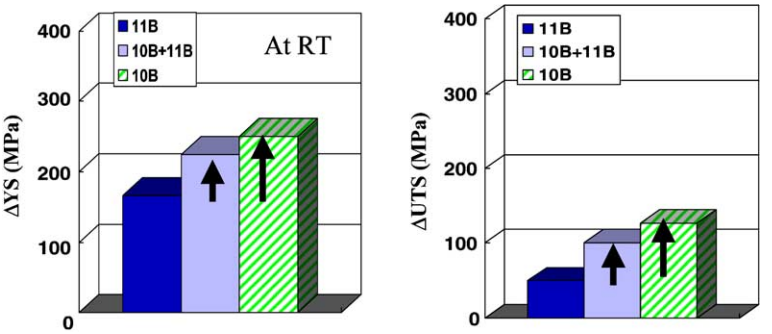

Fig. 6. Radiation hardening of yield strength and ultimate tensile strength due to B doping and He production in the specimens irradiated at 250 °C to 2.3 dpa.

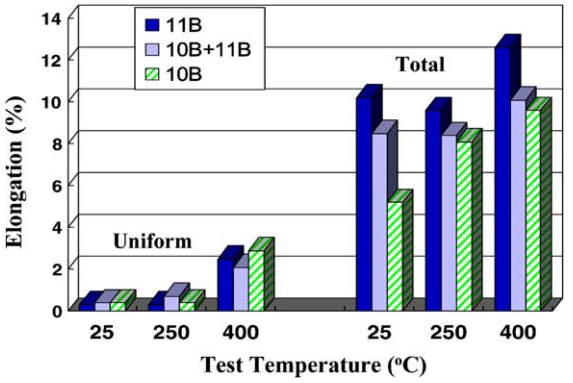

Fig. 7. Uniform and total elongations were degraded by irradiation at 250 °C to 2.3 dpa. The main cause of degradation was irradiation, however samples with 330 appm He show the largest degradation in total elongation.

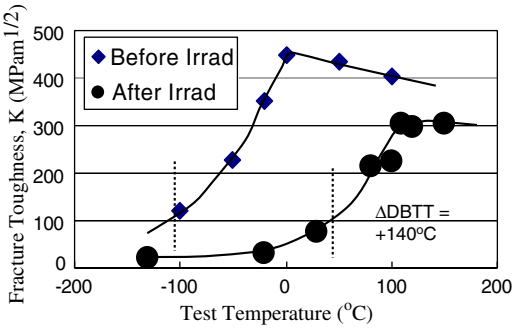

Fig. 8. Fracture toughness in the F82H + ^{11}B before and after irradiation.

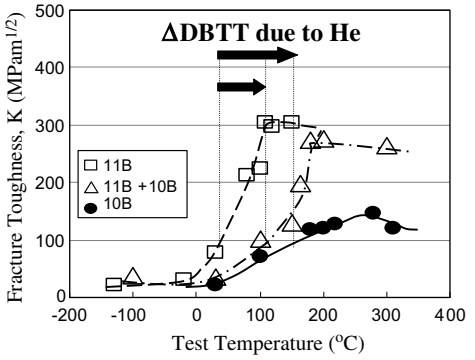

Fig. 9. Fracture toughness in the F82H + ^{11}B, F82H + ^{10}B + ^{11}B and F82H + ^{10}B specimens irradiated at 250 °C to 2.3 dpa.

temperatures of ductile regime, and it may be related to a high helium concentration.

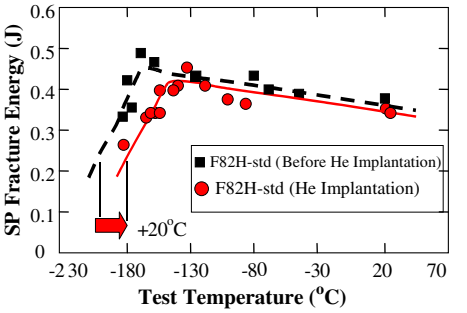

Fig. 10. SP fracture energies of F82H before and after He implantation as a function of temperature.

3.4. SP testing

SP energy was calculated from the area under the load–deflection curve up to the fracture load. The SP-results of the specimens implanted with about 85 appm He to 0.03 dpa and the non-implanted specimens are given in Fig. 10. The DBTT in the helium-implanted F82H steel was evaluated to be about 15 °C. The DBTT obtained by SP experiments was modified as 37.5 °C for the DBTT measured using a 1/3CVN standard as determined from the correlation between SP data and 1/3CVN (1/3 size Charpy specimen with V-notch) data [34]. The shift of DBTT due to displacement damage at 0.03 dpa can be evaluated from the other data of neutron irradiation experiment [9] and the value is estimated as about 5 °C. Therefore, the shift of DBTT due to helium production of 85 appm can be concluded to be 32.5 °C in the 1/3CVN. It was reported that the shift of DBTT obtained by 1/3CVN testing was coincided with that in the 0.18DCT testing [10].

3.5. SEM and EPMA

As reported in Refs. [35–37], Cr segregation is very sensitive to mechanical properties. The formation of α'-phase due to chromium segregation to sink sites can induce loss of ductility. If the concentration of Cr exceeds 12%, it is easy to occur phase separation of α and α'-phase during irradiation. Even in about 8%Cr alloys, α'-phase was observed on dislocation loops in the irradiated specimens. The formation of α'-phase is directly related to brittle property.

In Fig. 11, mapping images of Cr, C and B in the F82H + ^{11}B and F82H + ^{10}B were taken by the EPMA. No segregation of Cr at the fracture surface and boundaries such as lath boundaries was seen and the difference of the mapping images between F82H + ^{11}B and F82H + ^{10}B could not be detected. Therefore, the cause of the shift of DBTT is though to be the degradation of fracture energy due to trapping helium atoms at the boundaries of the package of lath martensitic structure.

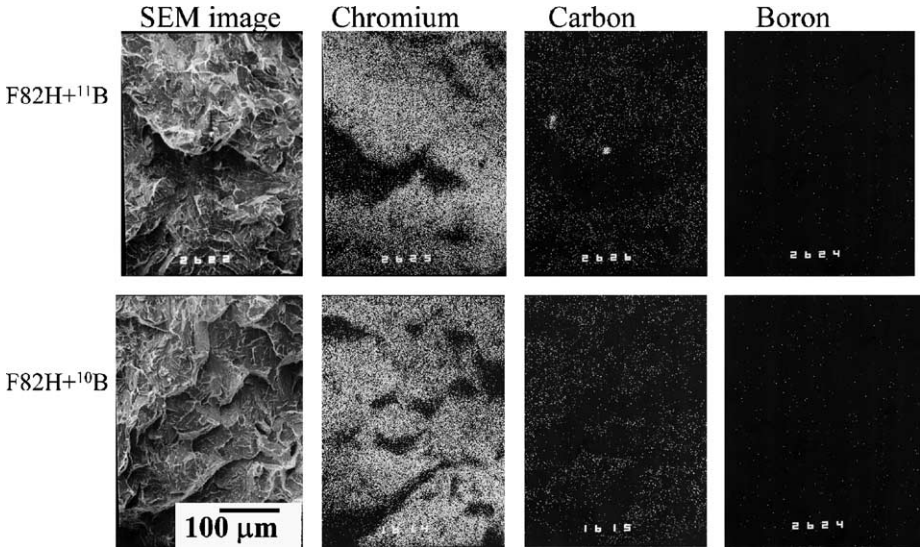

Fig. 11. SEM and EPMA mapping images of Cr, C and B after fracture testing of F82H + ^{11}B and F82H + ^{10}B.

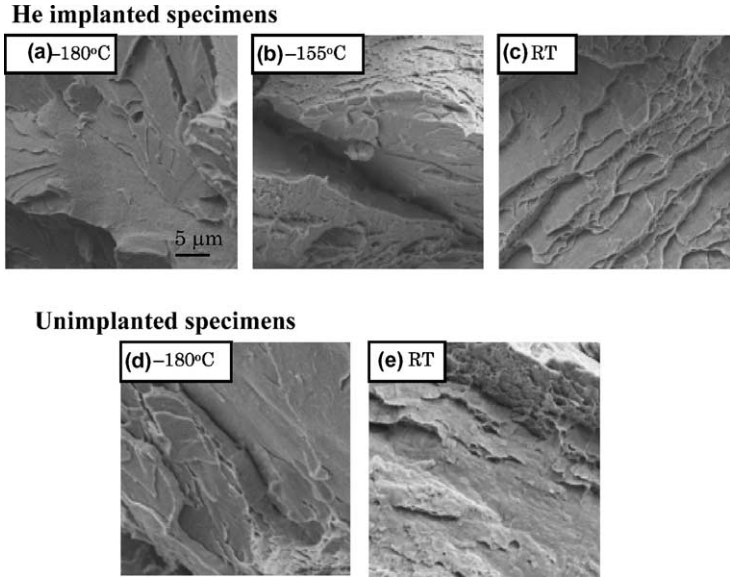

Fig. 12. Surfaces of F82H after SP testing in (a)–(c) He-implanted specimens and (d)–(e) no He-implanted specimens. Brittle fracture with like lath boundaries was formed in the F82H implanted with He ions (a).

Fig. 12(a)–(c) show the fracture surfaces taken by SEM for the 0.18DCT specimens of F82H + ^{11}B, F82H + ^{10}B + ^{11}B and F82H + ^{10}B steels after fracture testing performed at temperatures of brittle regime. In the F82H + ^{11}B steel, typical cleavage surfaces were observed as shown in Fig. 12(a). However, brittle fractures like lath boundary structure were formed in the F82H + ^{10}B + ^{11}B steel and brittle fractures with same smoothing surfaces were seen in the F82H + ^{10}B steel, as given in Fig. 12(b) and (c). According to Ref. [23], cavities were formed in dislocations and lath boundaries in only F82H + ^{10}B with a production helium about 330 appm in the specimens irradiated at 300 °C. Helium may be also trapped at sink sites such as lath boundaries in the specimen of this work.

SEM images after the SP fracture testing were given in Fig. 13. Similar structure in the brittle surface was observed in the SP specimen implanted with He atoms

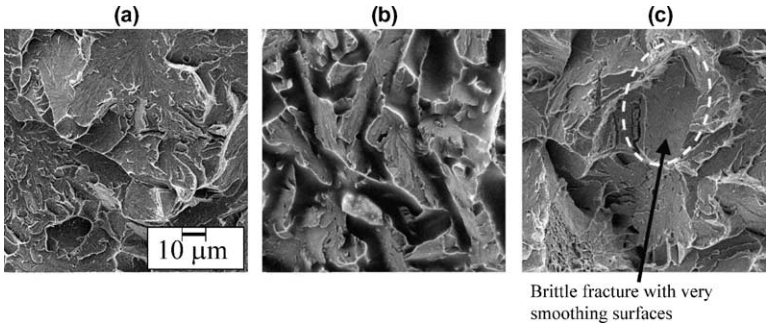

Fig. 13. Images of brittle fracture surface taken by SEM after fracture testing. (a) F82H + ^{11}B, (b) F82H + ^{10}B + ^{11}B and (c) F82H + ^{10}B irradiated by neutrons to 2.3 dpa.

after the testing as shown in Fig. 13(a). The size of transgranular areas was comparable to the package size of lath martensite in the specimen implanted with helium atoms, and the feature was not observed in the non-implanted specimens as seen in Fig. 13(d).

4. Discussion

4.1. Radiation hardening due to helium production

In Fig. 14, the change in yield stress of F82H steel induced by helium production is summarized as a function of helium production. ΔYS due to helium production, $\Delta YS(He)_1$, is defined as the difference between ΔYS of F82H + ^{10}B or F82H + ^{10}B + ^{11}B and ΔYS of F82H + ^{11}B and it is given by

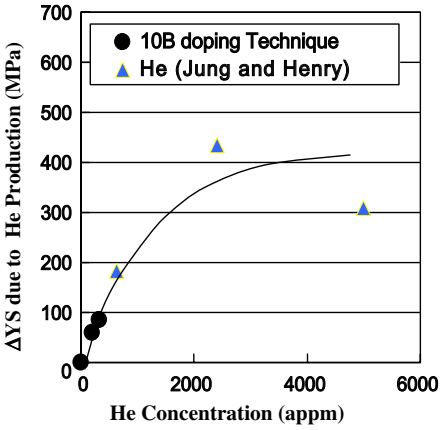

Fig. 14. Dependence of ΔYS on helium production in the F82H doped with isotope boron tested at room temperature. ΔYS due to helium production, $\Delta YS(He)_1$, is the difference between ΔYS of F82H + ^{10}B or F82H + ^{10}B + ^{11}B and ΔYS of F82H + ^{11}B. ΔYS due to helium production, $\Delta YS(He)_2$, is the difference of ΔYS between the helium implantation experiment of Jung [14] and neutron irradiation experiment of Abe [34].

$$\Delta YS(He) = \Delta YS(F82H + {}^{10}B \text{ or } F82H + {}^{10}B + {}^{11}B) - \Delta YS(F82H + {}^{11}B), \quad (1)$$

$$\Delta YS(F82H + {}^{10}B) = YS(F82H + {}^{10}B)_{irrad.} - YS(F82H + {}^{10}B)_{non\text{-}irrad.}, \quad (2)$$

where $YS_{irrad.}$ and $YS_{non\text{-}irrad.}$ are the yield stress of the specimen after and before irradiation. ΔYS induced by helium production is likely to continue the increasing somewhat at around 330 appm He. Similar results of radiation hardening due to helium production were reported by Jung and Henry [14,15] and the data of T91 martensitic steel implanted with helium were also plotted in Fig. 14. The ΔYS due to helium production, $\Delta YS(He)_2$, is the difference between the helium implantation experiment of Jung [14] and neutron irradiation experiment of Abe [38], and it is given by

$$\Delta YS(He)_2 = \Delta YS(\text{He implantation}) - \Delta YS(\text{neutron}), \quad (3)$$

$$\Delta YS(\text{He implantation}) = YS(T91)_{\text{He implantation}} - \Delta YS(T91)_{\text{non-impantation}}, \quad (4)$$

$$\Delta YS(T91) = YS(T91)_{irrad.} - YS(T91)_{non\text{-}irrad.}, \quad (5)$$

where ΔYS(He implantation) and ΔYS(neutron) are the increment of helium implantation and neutron irradiation at a same of displacement damage, respectively. The radiation hardening due to helium increases with increasing helium concentration up to about 2000 appm and it trends to saturate at a range from 2000 to 5000 appm. Henry observed the microstructures of T91 martensitic steel implanted with helium, and he showed that the main factor of hardening due to helium was caused by the formation of many cavities. The formation of cavities in the F82H + ^{10}B irradiated at 300 °C in HFIR was also observed [39], and it could be expected that the cavities would be also formed in this experi-

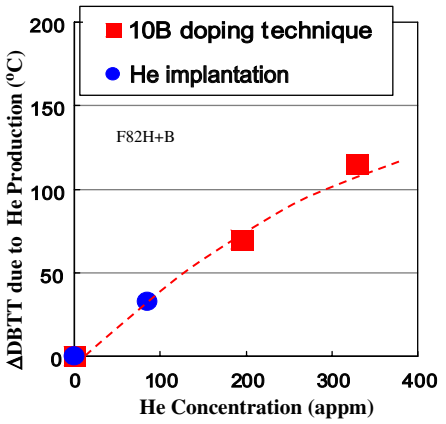

Fig. 15. Dependence of ΔDBTT on helium production in the F82H doped with isotope boron.

ment. Radiation hardening due to helium was also examined by experiments of single and dual ion beams [18], and it increased gradually with increasing helium concentration.

4.2. Radiation embrittlement due to helium production

In Fig. 15, the changes of ductile–brittle transition temperature in F82H steel induced by helium production are summarized as a function of helium production. ΔDBTT due to helium production, ΔDBTT(He), is defined as the difference between ΔDBTT of F82H + ^{10}B or F82H + ^{10}B + ^{11}B and ΔDBTT of F82H + ^{11}B and it is given by

$$\Delta\mathrm{DBTT(He)} = \Delta\mathrm{DBTT(F82H} + {}^{10}\mathrm{B \text{ or } F82H} + {}^{10}\mathrm{B} + {}^{11}\mathrm{B}) - \Delta\mathrm{DBTT(F82H} + {}^{11}\mathrm{B}). \quad (6)$$

ΔDBTT induced by helium production may also continue to increase for levels over 330 appm He. The effects of helium production and displacement damage on DBTT in ferritic/martensitic steels were reported by several researchers [5,9,10,16,29,30,40,41]. The DBTT of ferritic/martensitic steels depends on the chromium content, and other impurities and the formation of precipitates such as α′-phase [2,3,39,40] and M_6C [41]. A relatively large shift in DBTT, 70 °C, due to helium production about 20 appm was shown in a previous study using JLF-1 doped with natural boron [10], however the result did not take into account the chemical effect of boron on the shift in DBTT in the irradiated specimen and the real shift in DBTT should be a smaller value. Rieth [9] showed the dependence of the shift of DBTT due to helium production using several martensitic steels with different chromium concentration, and the ratio of the shift on DBTT to helium production was 2.5 °C/appm He. However the result includes the effect of chromium concentration on the shift in DBTT and the rate must be smaller value. In order to eliminate the chemical effect of doped element of Ni on the DBTT of martensitic steels to produce helium from a reaction of $^{58}\mathrm{Ni}(n,\gamma)^{59}\mathrm{Ni}(n,\alpha)^{56}\mathrm{Fe}$, Klueh compared the results of martensitic steels between the HFIR and EBR-II experiments, and the ratio of the shift in DBTT to helium production was relatively higher value of about from 1 to 4 °C/appm He [40].

In this study, the chemical effect of boron on DBTT was eliminated by using the isotope doping technique which compared the result for the specimens of F82H + 60 ppm ^{11}B, F82H + 30 ppm ^{10}B + ^{11}B + F82H + 60 ppm ^{10}B. We have to mention about the effect of the transmutation element of lithium produced from the reaction of $^{10}\mathrm{B}(n,\alpha)^{7}\mathrm{Li}$ on the shift in DBTT. Comparing the result of B-doped F82H of neutron irradiation with that of the non-B-doped F82H of the helium implantation experiments, it shows that the chemical effect of lithium on the shift in DBTT is very small as given in Fig. 15, and the effect of lithium on radiation hardening is also small as shown in Fig. 14. It may be necessary to perform a further investigation on the effect of lithium on DBTT in F82H. In this study, the enhancement of radiation hardening and the shift in DBTT is shown in the F82H steel irradiated at 250 °C to 2.3 dpa with helium up to about 330 appm He, however, the enhancement is reduced by increasing irradiation temperature at 300 °C [42]. This trend with increasing irradiation temperature matches with previous studies of Shiba and Rieth [5,9]. We need further information about the shift in DBTT due to helium production and have to continue the investigation of DBTT in martensitic steels with higher helium concentration from 330 to 1000 appm.

4.3. Model for the shift in DBTT due to helium production

In order to explain the shift of DBTT due to He production, the changes of yield stress and fracture stress before and after irradiation are shown in Fig. 16. DBTT can be recognized as a cross point between fracture stress curve and yield stress curve. In the figure the fracture stress 1 is shown to be constant during irradiation without helium production and fracture stress 2 is shown to be changed by the helium production during irradiation. T_{i} and T_{ii} are identified as DBTT before and after irradiation without helium production, respectively. T_{iii} and T_{iv} are identified as DBTT after irradiation with a synergistic effect of displacement damage and helium production under fracture stress 1 and 2, respectively. This experimental result of DBTT shift due helium production indicates that T_{iv} is adequately greater than T_{iii}. The reason of the fracture stress 2 is described as below: (1) the shift of DBTT due to helium

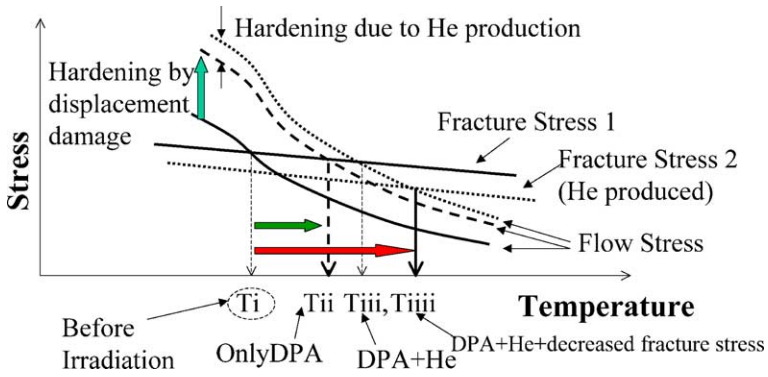

Fig. 16. Explanation of ΔDBTT due to He production.

production was relatively large; (2) the fracture surface after the fracture testing at temperature of brittle regime was not simple cleavage surface and had a structure like lath boundary or smoothing cleavage surface as shown in Fig. 12; (3) the ratio of fracture strength to fracture area in tensile testing in the irradiated F82H + ^{10}B steel was about 40% smaller than that in the irradiated F82H + ^{11}B steel. Therefore, the shift of DBTT due to helium production can be explained by the decrease of fracture stress.

In Fig. 17, the mechanism of the dependence of the shift of DBTT due to helium production on dpa is shown. The shift of DBTT due to helium production on dpa can be explained by radiation hardening and degradation of fracture stress. The mechanism of the dependence of the shift of DBTT on irradiation temper-

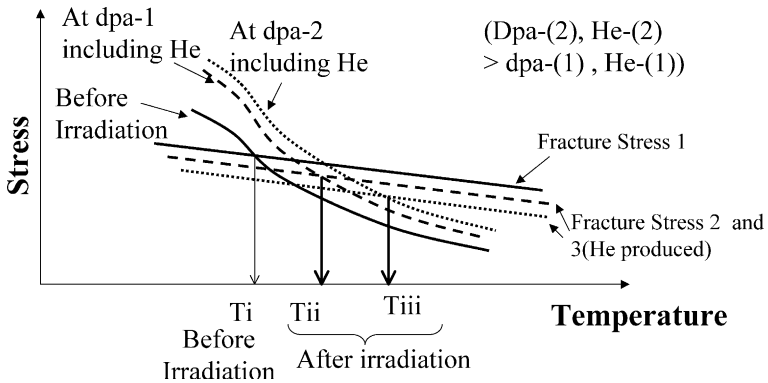

Fig. 17. Dependence of ΔDBTT due to He production on displacement damage.

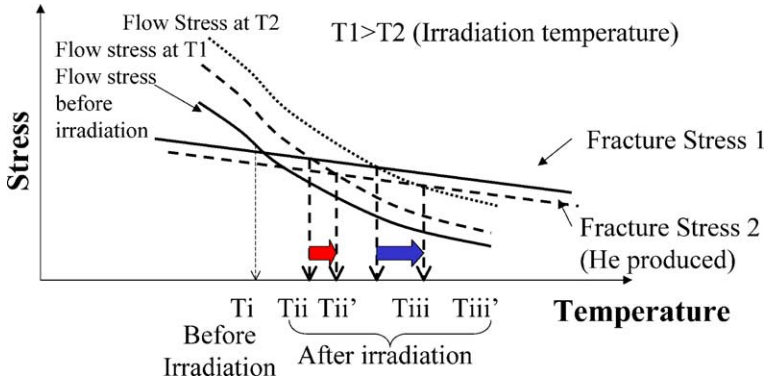

Fig. 18. Dependence of ΔDBTT on irradiation temperature.

ature is also given in Fig. 18. The shift of DBTT due to helium production at T1 (higher temperature) will be smaller than that at T2 (lower temperature) under the fracture stress 2.

4.4. Role of helium, hydrogen and displacement damage on the mechanical properties and microstructures

The synergistic effect of helium, hydrogen and displacement damage on microstructures in ferriitc/martensitic steels was reported in Refs. [22–26], and swelling was enhanced by the synergistic effect of helium and hydrogen [22–24]; the hardness changes obtained by ion irradiation experiments were reported [18,25,26] and the enhancement effects of gas elements were reported. On the other hand, Dai reported that enhancement of synergistic effect of helium, hydrogen and displacement damage on radiation hardening and the shift in DBTT was not observed up to 565 appm He, 3500 appmH and 7.6 dpa in the spallation target experiment and occurred at 815 appm He, 4400 appmH and 9.8 dpa in the spallation target experiment [29,30]. The result obtained in this study is different from the spallation target result, and the behavior of changes of radiation hardening under the existence of helium and hydrogen atoms is very complex and further investigation will be necessary.

5. Conclusion

The dependence of helium production up to about 330 appm on hardening and embrittlement has been examined in F82H steel irradiated at 250 °C to 2.3 dpa by tensile and fracture toughness tests. The increments of yield and ultimate tensile stresses by irradiation tended to increase slightly with increasing helium production. The shifts of ductile brittle transition temperatures due to helium production were evaluated as about +70 °C by 190 appm He and +115 °C by 330 appm He, respectively in a JMTR experiment using boron-doped F82H steels. In a cyclotron experiment using standard F82H, a similar DBTT shift due to He was measured. These results suggest that helium production can increase the DBTT.

Acknowledgement

The authors would like to express sincere thanks to staffs of hot laboratory of JMTR, JMTR operation in Oarai establishment of JAERI and TIARA facility in Takasaki establishment of JAERI. The measurements of He concentration in the specimens were performed in the Nuclear Development Company of Tokai-mura.

References

[1] R.L. Klueh, M.A. Sokolov, K. Shiba, Y. Miwa, J.P. Robertson, J. Nucl. Mater. 283–287 (2000) 478.
[2] E. Wakai, A. Hishinuma, K. Usami, Y. Kato, S. Takaki, K. Abiko, Mater. Trans., JIM 41 (9) (2000) 1180.
[3] E. Wakai, A. Hishinuma, T. Sawai, S. Kato, S. Isozaki, S. Takaki, K. Abiko, Phys. Status Solidii (a) 160 (1997) 441.
[4] K. Shiba, A. Hishinuma, J. Nucl. Mater. 283–287 (2000) 474.
[5] K. Shiba, I. Ioka, J.P. Robertson, M. Suzuki, A. Hishinuma, Euromat-96 (1996) 265.
[6] A.F. Rowcliffe, J.P. Robertson, R.L. Klueh, K. Shiba, D.J. Alexander, M.L. Grossbeck, S. Jitsukawa, J. Nucl. Mater. 258–263 (1998) 1275.
[7] S.J. Zinkle, J.P. Robertson, R.L. Klueh, Fusion Reactor Materials Semiannual Progress Report for Period Ending 30 June 1998, Office of Fusion Energy, DOE/ER-0313/24, 1998, p. 135.
[8] E.I. Materna-Morris, M. Rieth, K. Ehrlich, Effects of radiation on materials, STP1366, 2000, p. 597.
[9] M. Rieth, B. Dafferner, H.-D. Rohrig, J. Nucl. Mater. 258 (1998) 1147.
[10] Emile van Osch, M. Horsten, G.E. Lucas, G.R. Odette, Effects of radiation on materials, STP1366, 2000, p. 612.
[11] N. Yamamoto, N. Yamamoto, J. Nakagawa, K. Shiba, J. Nucl. Mater. 283–287 (2000) 400.
[12] Y. Dai, S.A. Maloy, G.S. Bauer, W.F. Sommer, J. Nucl. Mater. 283–287 (2000) 513.
[13] N. Baluc, R. Schaublin, C. Bailat, F. Pashoud, M. Victoria, J. Nucl. Mater. 283–287 (2000) 731.
[14] P. Jung, J. Henry, J. Chen, J.-C. Brachet, J. Nucl. Mater. 318 (2003) 241.
[15] J. Henry, M.-H. Mathon, P. Jung, J. Nucl. Mater. 318 (2003) 249.
[16] R.L. Klueh, J.M. Vitek, J. Nucl. Mater. 150 (1987) 272.
[17] L.K. Mansur, M.L. Grossbeck, J. Nucl. Mater. 155–157 (1988) 130.
[18] M. Ando, E. Wakai, H. Tanigawa, T. Sawai, K. Furuya, S. Jitsukawa, H. Takeuchi, K. Oka, S. Ohnuki, A. Koyama, J. Nucl. Mater. 329–333 (2004) 1137.
[19] A. Kimura, T. Morimura, R. Kasada, H. Matsui, A. Hasegawa, K. Abe, Effects Radiat. Mater. STP 1366 (2000) 626.
[20] A. Kimura, R. Kimura, K. Morishita, R. Sugano, A. Hasegawa, K. Abe, T. Yamamoto, H. Matsui, N. Yoshida, B.D. Wirth, T.D. Rubia, J. Nucl. Mater. 307–311 (2002) 521.
[21] Y. Katoh, M. Ando, A. Kohyama, J. Nucl. Mater. 323 (2003) 251.
[22] E. Wakai, K. Kikuchi, S. Yamamoto, T. Aruga, M. Ando, H. Tanigawa, T. Taguchi, T. Sawai, K. Oka, S. Ohnuki, J. Nucl. Mater. 318 (2003) 267.
[23] E. Wakai, T. Sawai, K. Furuya, A. Naito, T. Aruga, K. Kikuchi, S. Yamashita, S. Ohnuki, S. Yamamoto, H. Naramoto, S. Jitsuakawa, J. Nucl. Mater. 307–311 (2002) 278.
[24] T. Tanaka, K. Oka, S. Ohnuki, S. Yamashita, T. Suda, S. Watanabe, E. Wakai, J. Nucl. Mater. 329–333 (2004) 294.
[25] E.H. Lee, J.D. Hunn, G.R. Rao, R.L. Klueh, L.K. Mansur, J. Nucl. Mater. 271&272 (1999) 385.

[26] J.D. Hunn, E.H. Lee, T.S. Byun, L.K. Mansur, J. Nucl. Mater. 296 (2001) 203.
[27] J. Henry, X. Averty, Y. Dai, P. Lamagnere, J.P. Pizzanelli, J.J. Espinas, P. Wident, J. Nucl. Mater. 318 (2003) 215.
[28] M.B. Toloczko, M.L. Hamilton, S.A. Maloy, J. Nucl. Mater. 318 (2003) 200.
[29] Y. Dai, X.J. Jia, K. Farrell, J. Nucl. Mater. 318 (2003) 318.
[30] X.J. Jia, Y. Dai, J. Nucl. Mater. 323 (2003).
[31] K. Farrell, T.S. Byun, J. Nucl. Mater. 318 (2003) 274.
[32] Y. Miwa, T. Tsukada, Y. Nakanura, S. Hamada, H. Tsuji, JAERI Rev. 97-015 (1997) 108.
[33] G.E. Lucas, G.R. Odette, K. Edsinger, B. Wirth, J.W. Sheckherd, 17th International Symposium on Effects of Radition on Materials, ASTM STP 1270, 1996, p. 790.
[34] M. Eto, H. Takahashi, T. Misawa, M. Suzaki, Y. Nishiyama, K. Fukaya, S. Jitsukawa, Small specimen test techniques applied to nuclear reactor vessel thermal annealing and plant life extension, ASTM STP 1204, 1993, p. 241.
[35] E. Wakai, A. Hishinuma, Y. Kato, H. Yano, S. Takaki, K. Abiko, J. Phys. IV C7 (1995) 277.
[36] E. Wakai, A. Hishinuma, Y. Miwa, A. Ouchi, S. Isozaki, S. Takaki, K. Abiko, Mater. Trans. JIM 41 (1) (2000) 136.
[37] E. Wakai, A. Hishinuma, M. Asahina, Y. Miwa, K. Mitsuishi, M. Song, S. Takaki, K. Abiko, Phys. Status Solidii (a) 189 (1) (2002) 79.
[38] F. Abe, M. Narui, H. Kayano, Mater. Trans., JIM 34 (1993) 1053.
[39] E. Wakai, Y. Miwa, N. Hashimoto, J.P. Robertson, R.L. Klueh, K. Shiba, K. Abiko, S. Furuya, S. Jitsukawa, J. Nucl. Mater. 307–311 (2002) 203.
[40] R.L. Klueh, J. Nucl. Mater. 218 (1995) 151.
[41] P. Dubusson, D. Gilbon, J.L. Seran, J. Nucl. Mater. 205 (1993) 178.
[42] E. Wakai, S. Jitsukawa, H. Tomita, F. Takada, J. Nucl. Mater., submitted for publication.